UCLA Wind Project
Turbine Design Report
2022-2023 Collegiate Wind Competition
May 4, 2023

Turbine Design Team:

Aki Takahashi

Alyssa Gee

Amos Ancell (Mechanical Lead)

Ben Vivier

Eva Fiedler (Electrical Lead)

Jared Norton

Jeremy Keast

Julia Chow

Kirsten Wannenwetsch

Lee Moyer

Sakshi Agte

Sam Berman

Zack Figueroa (Project Manager)

Faculty Advisor: Sam Taira

Table of Contents

1.0 Executive Summary

As anthropogenic greenhouse gas emissions impact the global climate, offshore wind becomes an increasingly significant aspect of emission reduction plants. This report details the engineering design of a small-scale wind turbine created by UCLA Wind Project for the Department of Energy's Collegiate Wind Competition (CWC). The short-term project goal was to build a safe and working turbine that can perform successfully in the CWC Turbine Testing tasks while the long-term goal was to encourage and prepare students for a career in renewable energy. The design of the turbine is split into two main subsystems: the mechanical system,

which broadly consists of the blades/pitch control, nacelle/tower, and foundation, and the electrical subsystem, which consists of the generator, a power system, and a control system.

The primary consideration for blade design was the airfoil selection, spanwise chord and twist distributions. Publicly available airfoil data was gathered in Python and analyzed using the open-source QBlade software to optimize the capacity of our wind turbine. Complementing the blades is a pitch control system, the most technically nuanced part of the mechanical subsystem, which pitches and feathers the blades to control power production. The pitch control system has a maximum pitching angle of 72° and limits rotational speed and power production at wind speeds above 11 m/s and can provide full shut-down capabilities during emergency conditions. On the other end of the turbine, the foundation features a tripod design with piles and helical augers to engage the sand. A tripod design was chosen to ensure structural integrity under cyclic loads from typical wind turbine operation and the potentially large impulsive loads from the shutdown process and other extreme environments.

The electrical system was designed with the goal of maximizing power and providing safe shutdown scenarios while keeping the design as simple as possible. Two latching relays enable redirection of power through the point of common coupling (PCC) from turbine to load and load to turbine, depending on the mode of operation. A linear actuator control board is used to control pitch angle during active pitching in the power regulation state, and pitching between normal pitch and braking pitch. A single resistance load was chosen to simplify the load design. Two Arduino microcontrollers control relay state and pitch angle based on mode of operation and communicate through optically-isolated connection.

1.1 Design Objective

The primary objective of the project was to design and manufacture a small wind turbine that resembles a fixed-bottom offshore wind turbine while conforming to the CWC's rules and regulations. Specific objectives included maximizing power at 11 m/s, controlling power and rotational speed above 11 m/s, and enabling a shutdown procedure that could be initiated on command or upon load disconnect. The airfoil selection and blade design primarily targeted maximizing power at 11 m/s and the pitch control system primarily targeted the control of rated power and shutdown procedures. As this is the first year that UCLA is participating in the CWC, we drew significant inspiration from successful teams in past years, particularly Kansas State University in 2022. Discussions with the 2021 Cal Maritime aerodynamics team provided the insight that good airfoils should not just have a high maximal glide ratio but should have a high mean glide ratio in a neighborhood around that maximum. Furthermore, our stress-testing method for the blades comes directly from Pennsylvania State University's past reports. Our pitch control design drew on many schools' past reports, particularly University of Wisconsin-Madison. Inspiration for factors to consider in generator selection came from Virginia Tech.

2.0 Blade Design

2.1 Airfoil Selection

A three-blade rotor was designed using QBlade. Each blade has a spanwise length of roughly 16cm, made using three airfoils: GOE 430 near the root, GOE 57 near the tip, and a 50%

interpolation between the two for the middle. Using Python, webscraped data on glide ratios (Cl/Cd) versus angle of attack (AOA) at Reynolds number 50,000 was collected for over 1,600 airfoils (Figure 1). After a literature review, it was evident that root airfoils would need high thickness for desired structural integrity. The GOE 430 was selected for this reason, in addition to its high glide ratio at low AOAs compared to other thick airfoils. The GOE 57 was chosen for its high maximum Cl/Cd and mean Cl/Cd around that maximum. High mean Cl/Cd near peak is desired as many blade sections will not operate exactly at their maximizing AOA, so a high Cl/Cd near that AOA can still result in generally high glide ratios. The 50% interpolation was chosen to smoothly transition between the two airfoils and prevent focal points of stress when the airfoils change. Chord and twist distributions were optimized for a TSR of 3.5, which has a peak power coefficient (Cp) of approximately 0.36. Cp represents how efficiently a turbine converts the energy in the wind to electricity (Figure 2).

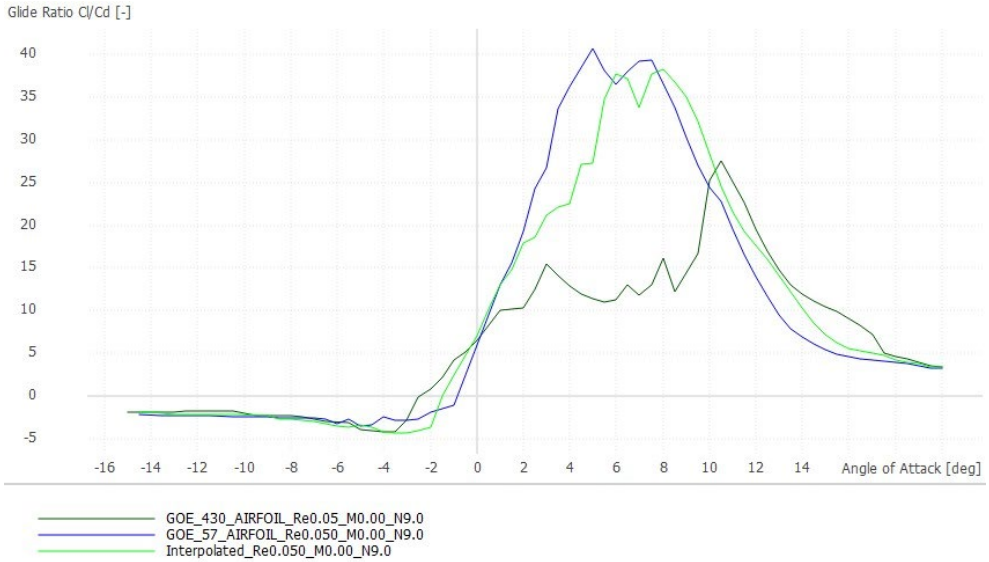

Figure 1: Angle of Attack vs. Glide Ratio

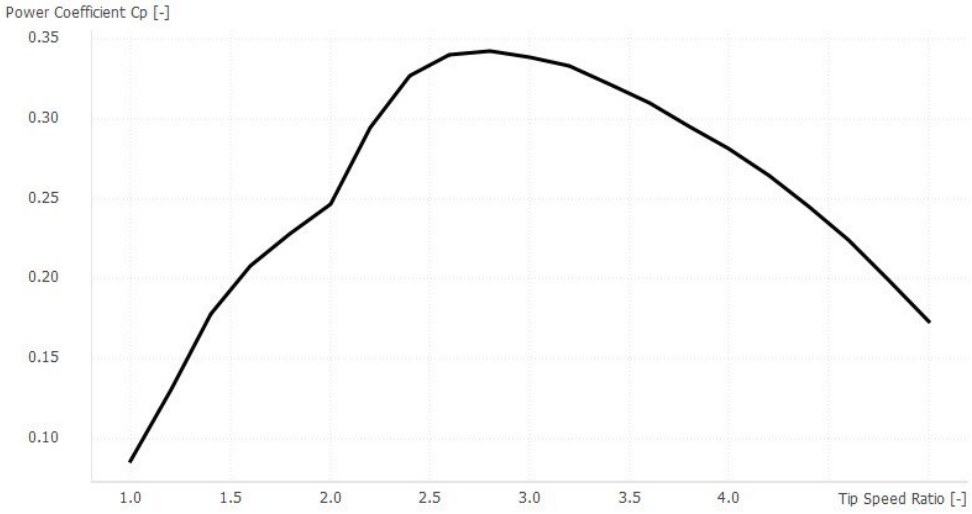

Figure 2: TSR vs. Power *Coefficient*

The connection between the rotor hub and the blade was iterated to ensure our pitch control mechanism would work in tandem. Specifically, we designed the connection such that the leading edge of the blade was nearly parallel to the wind direction near maximum actuation. One concern that arose was the actuator piston nearly coming into contact with the blade during operation. The connection piece was therefore also adjusted based on this design constraint, which required several iterations for a satisfactory design.

2.2 Blade Manufacturing

We fabricated our blades by 3D printing them with fused deposition modeling technology on a MakerBot Replicator+ printer using PLA at a resolution of 100 microns and 100% infill. A high infill percentage was needed for structural integrity and the connection between the rotor hub and blade was designed to have a flat profile so that 3D printing was viable. Consideration was given to casting the blades with molds, but 3D printing was chosen instead to permit rapid iteration, something we deem especially critical for us as a young team. The blade was printed in the orientation shown in Figure 3 to ensure the best finish across the airfoils, with minimal supports around the connection between the rotor hub and blade. Despite these measures, the first iterations of the blades had poor finish and rough leading and trailing edges. Consequently, fabrication was also considered using a Formlabs Form 2 printer which uses stereolithography technology and has four times the resolution of the MakerBot Replicator+.

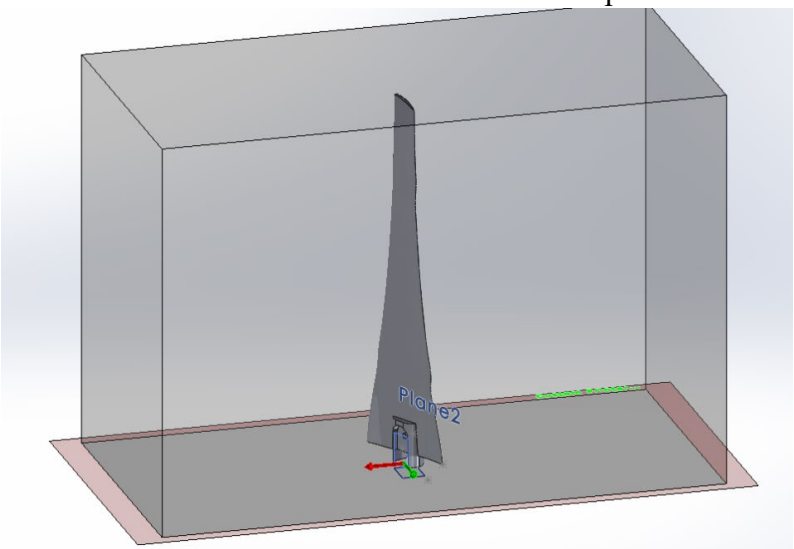

Figure 3: Model of our blade with rotor attachment

2.3 Blade Testing

To test the individual blades' structural integrity, the blades were placed in a table vice and a series of increasingly heavy weights were hung from the blade tips while measuring tip deflection. During this process we also took note of signs of fracturing or breaking, of which there were none. The heaviest weight was 1992 g corresponding to a force of ~20 N applied to the blade tip. The blade did not break under this load and as this force is much higher than expected forces during competition, we are confident in the current blades' structural integrity.

Table 1: Blade Stress Test Data

Weight (g)	Tip Deflection (cm)	Signs of breaking?	Force (N)
202	0.7	none	1.98
530	1.7	none	5.20
733	2.3	none	7.19
1110	3.6	none	10.89
1312	4.7	none	12.87
1517	6.5	none	14.88
1992	7.7	none	19.54

2.4 Pitch Control

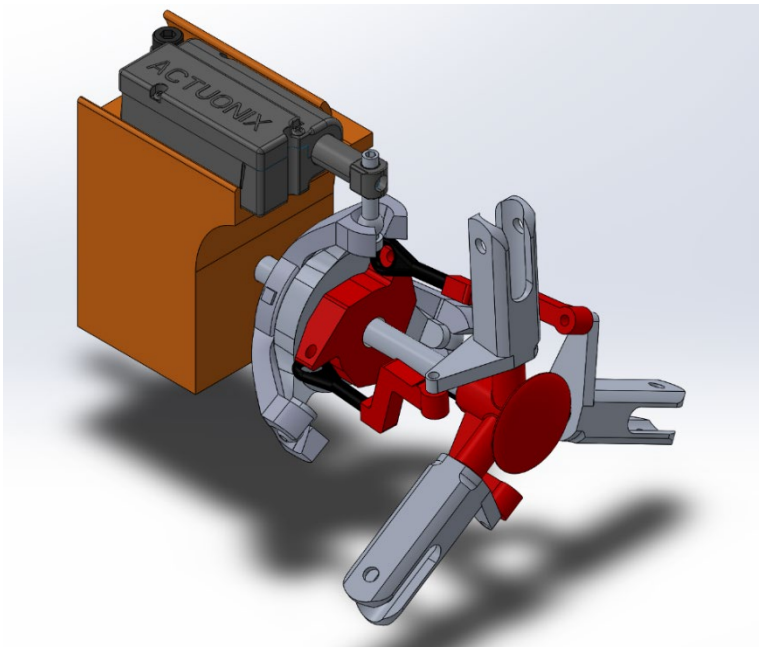

Figure 4: Pitch control assembly, including the RC rotor set, pitch control slider, linear actuator and its mount.

The pitch control mechanism on the turbine combines both outsourced and machined in-house components (Figure 4). A T-Rex RC 450 Helicopter Rotor Head Set was purchased to provide a convenient and reliable pitch control mechanism. A handmade CAD model of the helicopter rotor assembly was designed to ensure the connecting parts would be compatible. The size of the rotor had to be small enough to meet the size requirements of the turbine while also being large enough so that the blades would not interfere with each other. The pitching mechanism uses an Actuonix PQ12-P Micro Linear Actuator with Feedback. This actuator has multiple gearing options, including 30:1, 63:1, and 100:1 gear ratios. The 100:1 gear ratio was

chosen as it can resist the largest back drive force (up to 35 N) of the three types. The turbine needs to withstand a back drive force because the blades can pitch backwards and disrupt the pitch control's programming if the force of the wind is too great. The actuator has a stroke length of 20 mm; as it actuates, the attached base plate and the three linkages connecting the base plates to the blade holsters move forwards and rotate the holsters, which pitches the blades.

A trigonometric calculation was done to determine the maximum pitching angle (Figure 5). With a stroke length of 20 mm, and a length of 17 mm between the linkage-blade holster joint axis and the blade insertion axis, the pitching angle could be determined.

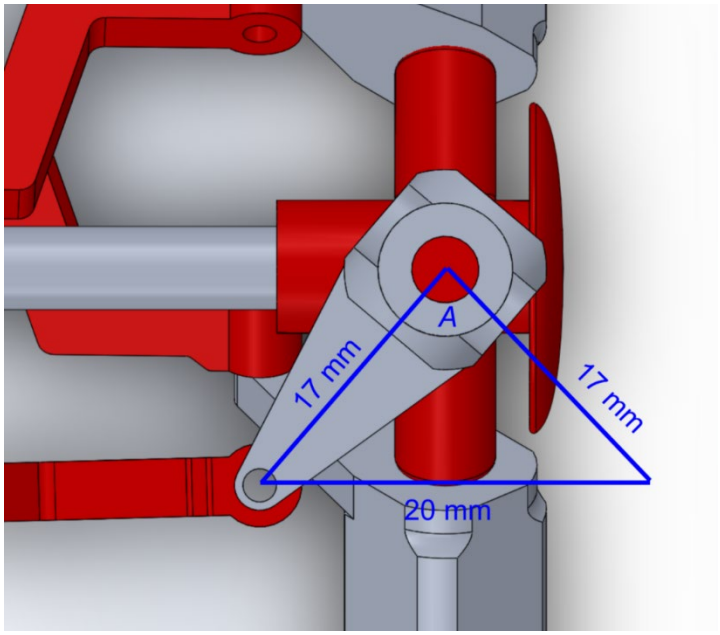

Figure 5: Maximum pitching angle of blades.

$$A = 2\sin^{-1}\left(\frac{10}{17}\right) = 72°$$

The maximum pitching angle the blades can achieve is 72°, which was verified through SolidWorks measurements. To produce a maximum pitching angle of 90°, the stroke length of the actuator would need to be at least 24 mm. A pitching angle of 90° is used to feather the blades when the wind speeds surpass the turbine's rated wind speed. A pitching angle of 0° is desirable during low wind speeds to maximize the turbine's power.

Additionally, we designed a pitch control slider that attaches to the swashplate that limits the degrees of freedom of the rotor. The slider is 3D printed with PLA to ensure the part was easily manufactured. The initial design was iterated several times as the snapping mechanism would often break when attaching the slider to the swashplate. The upright printing orientation of the slider greatly contributed to its fragility in earlier iterations because the shear stresses were concentrated between the PLA layers. To fix this issue, the thickness of the snapping mechanism

was significantly increased to reduce the shear stress. The finalized design of the slider is shown in Figure 6.

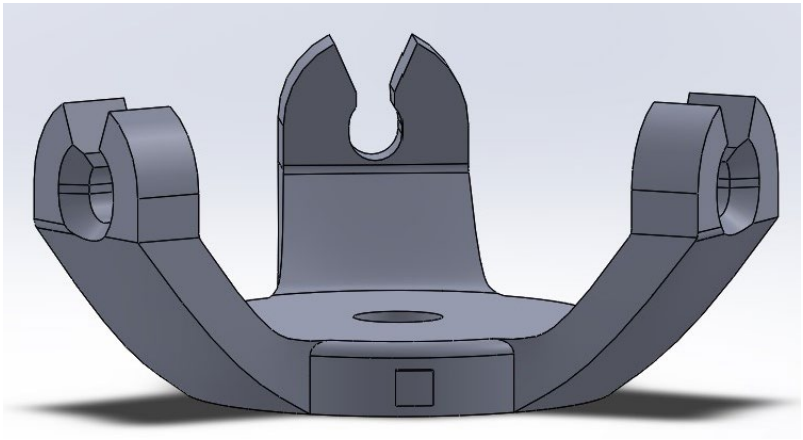

Figure 6: Final design of Pitch Control Slider.

The platform that holds the linear actuator was also 3D printed in PLA and sits on the nacelle. The platform doesn't interfere with the turbine's shaft and contains M3 threaded brass heat set inserts that connect both the actuator to the platform and the platform to the base of the nacelle.

To confirm that the swashplate's motion was confined to translation along the rotor axis, the swashplate and slider were actuated back and forth to ensure that the slider remained connected to the swashplate. After verifying the pitch control slider effectively reduced the degrees of freedom of the rotor, we tested our subassembly in a wind tunnel at various wind speeds. During this wind tunnel testing, data on power output and rotational speed at various wind speeds were measured and collected into a database. This database was then used to calibrate our actuator and develop a program that limits power production and rotational speed at wind speeds above 11 m/s to avoid runaway power.

3.0 Nacelle and Tower

3.1 Design and Simulation

Preliminary turbine structure testing was performed via FEA analysis in SolidWorks to ensure that the tower can withstand a wind speed of 22 m/s. Wind pressure was estimated as $PP = 0.613V^2$ [1]. In the FEA simulation, a circle depicting the swept area of the blades was used and a load was applied to the frontal area of this circle (Figure 7). The minimum factor of safety from this simulation was 18, suggesting that wind induced stress is not an urgent issue for structural integrity. The factor of safety was roughly uniform along the entire turbine, another positive sign.

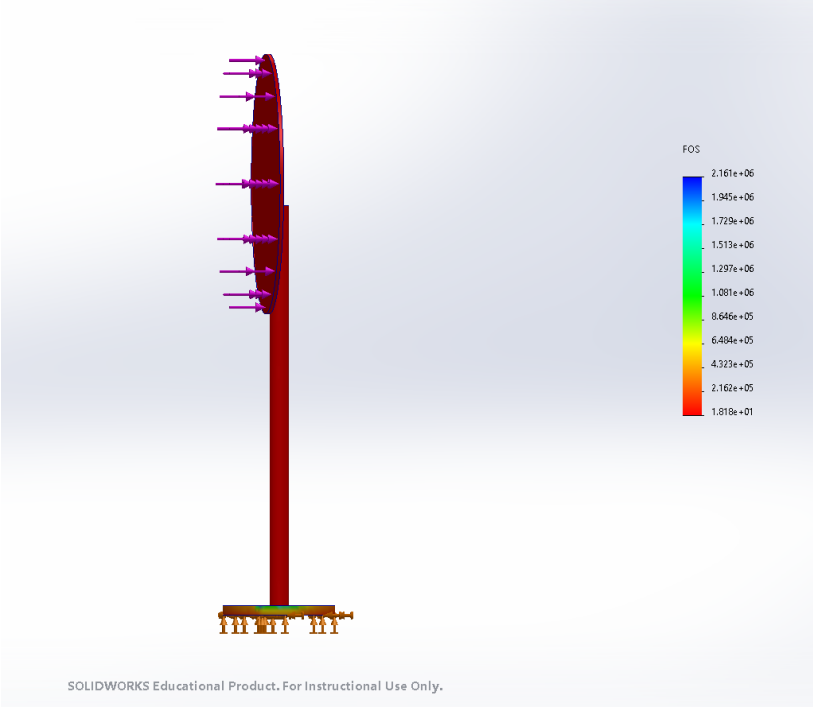

Figure 7: Factor of safety distribution for circular wingspan.

3.2 Tower Manufacturing

The nacelle and tower clamp were 3D printed in PLA to allow for quick fabrication. The tower began as a 3 ft 1” diameter rod and was cut down to ~54 cm using a horizontal bandsaw. The base plate began as a 15.4 cm diameter 1⁄2” thick aluminum disc and had holes drilled in it using a mill. For assembly, the base plate is welded to the tower and components are added to the top of the tower in the following order: tower clamp, bearing mount, nacelle. Each component is locked in with 2 nuts and bolts. During assembly in the wind tunnel, a circular worm-drive clamp around the tower clamp will lock yaw rotation once the turbine is oriented in the direction of the wind.

3.3 Tower Clamp & Bearing

The competition does not call for either active or passive yaw control, but the turbine still must be capable of orienting towards the wind during installation, so it needs to also lock in place once set. To achieve this, a bearing mount was attached to the tower and the nacelle, allowing the nacelle to rotate around the tower. A 3D printed clamp was additionally placed around the tower and a worm-drive clamp is used for tightening the clamp to the tower. When tightened, the friction between the clamp and the tower prevents rotation of the nacelle. The worm-drive can endure a maximum torque of 80-pound-force-inches, and testing in the wind tunnel demonstrated it could handle this level of force.

For competition, the turbine will enter the tunnel with the worm-drive loosened so that the turbine can be installed with the blades in the direction of the wind. Once the direction is established, the worm drive is tightened, locking the nacelle in the proper direction.

3.4 Nacelle

The nacelle was divided into two pieces: the base and the shell. The base was a 1-cm thick 3D-printed piece, that had four screw holes to hold the pitch control mount, as well as a cut out for the generator to fit into (Figure 8). The cut out prevents lateral motion of the generator and the back wall that covers the generator encoder prevents rotational motion. If there had been more time to iterate the design before testing and competition, an additional fit to prevent vertical motion would have been added. However, once connected to the pitch assembly, the generator is secure and there are no forces that would be expected to cause vertical motion.

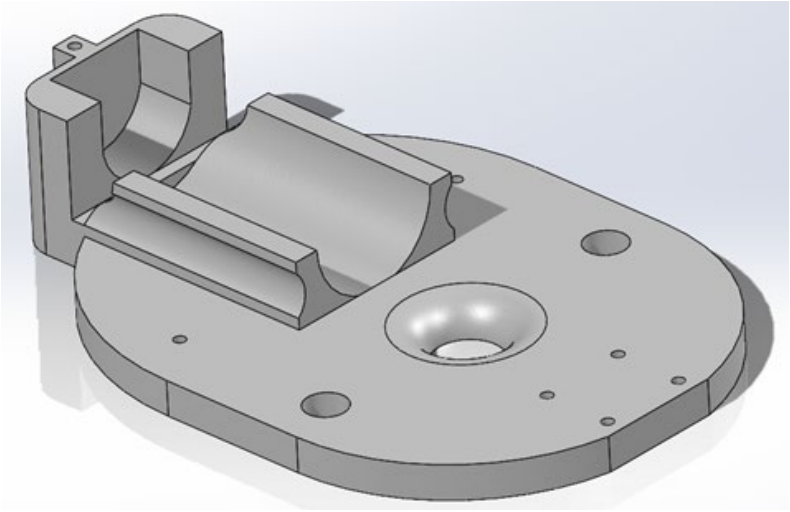

Figure 8: Image of the base of the nacelle in SolidWorks.

Additionally, two nuts and bolts connect and hold the nacelle baseplate to the bearing mount and tower clamp. For the shell, shown in Figure 9, the design emphasis was protecting the electronics from external wind. Because there was a delay in materials arriving, it was challenging to iterate the most optimized design while ensuring sufficient time to test. For this reason, the shell was a simple, 3D printed housing that connects with the nacelle base via similar screw holes to the pitch assembly located on either side and the back. The shell is designed so that there is adequate space for the electronics to fit inside and allows wires to run down the tower center.

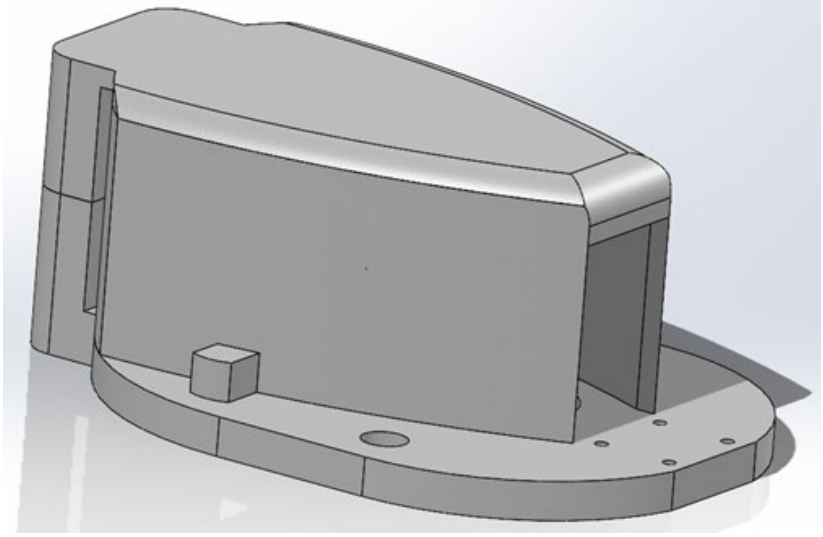

Figure 9: The shell housing on the base of the nacelle in SolidWorks.

4.0 Foundation

4.1 Foundation Design and Considerations

The foundation features a tripod design with piles and helical augers to engage the sand for installation and support. Initially, the legs on the tripod were angled downward, but due to complexity in manufacturing, the design was altered to straighten the legs (Figure 10). A tripod design is favored over a jacket design because it provides similar lateral loading support without as significant an increase in design and manufacturing complexity. In contrast, monopiles are simple but require significant force to insert into sand and a relatively large diameter to provide necessary stability, in turn increasing the foundation's weight [2]. Helical piles were chosen because they withstand tensile loading well, can be used in a variety of sand types, and facilitate easy installation [3]. The "screw" aspect makes them easier to install than driving a standard pile into the sand, which in turn requires less equipment. It would also be quieter than pile driving, which is important consider in regards to wildlife.

4.2 Foundation Fabrication

For fabrication, all tubes (center, tripod legs, and screw holders, made from 4130 steel alloy) were cut down to size using a horizontal bandsaw. Then the tripod legs were contoured using an end mill of diameter equal to that of the center tube and screw holder. While milling the contours into the tripod legs, the center tube was included in the vice setup. This ensured that the legs stayed flush to the center tube during machining, so that the orientations of the contours would remain parallel. The augers were created by welding a circular steel plate (low carbon steel alloy) onto a shaft of 18-8 stainless steel. The circle was cut using a CNC machine and cut into with a bandsaw to create a slit. In doing so, the circle could be bent to the desired pitch to create the screw. To assemble the remaining parts, the tripod legs were welded onto the center tube, and the base screw holders and the augers were welded onto their shafts.

Prior to competition, screw shafts will be inserted into the base screw holders and 1-2 hex nuts will secure them. During competition, the assembly will be set in the competition tank and a

wrench used to screw the augers into the sand. A level will be used once parts are screwed into place to ensure the foundation is straight. In order to make full use of the length of the auger support and ensure a stable insertion into the sand, a 1.5” steel tube will be placed over the auger shaft to rest on the augers and act as a stop. The full assembly can be seen in Figure 11.

4.3 Foundation testing

During testing, the foundation was simple to install: the auger shaft was placed through the stops and auger holders and the hex nuts were threaded on. Then the assembly was placed in the tank and the auger shafts rotated to screw the foundation firmly into the sand. This structure achieved a stable hold when force was applied to the center column.

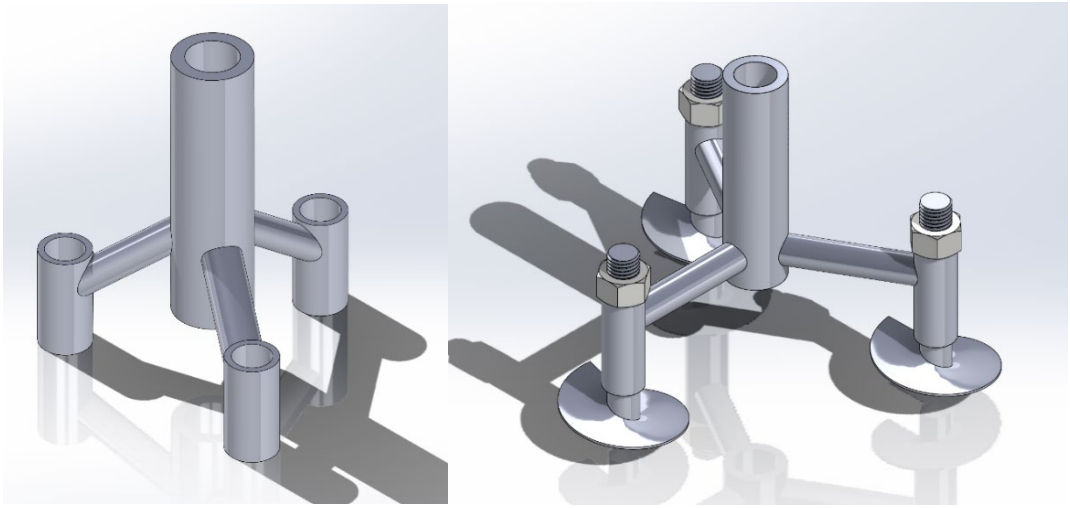

Figure 10: Design change from angled tripod legs (left) to straight (right).

Figure 11: Fully assembled foundation, with augers, stops, and hex nuts attached.

5.0 Electrical System Design

5.1 Generator Choice

The generator chosen was the graphite brushed 150 Watt Maxon RE 40 motor (part no. 218010) (Figure 12). A brushed DC motor was chosen as a generator over an AC motor or brushless DC motor to avoid the need for rectification. The usual concerns of low efficiency and commutator brush wear in DC generators were less of a concern due to the wind turbine's small size and short required life-span.

Figure 12: Maxon RE 40 Brushed DC Motor.

During the generator selection process, the expected performance of several Maxon DC motors were compared. In order to estimate the maximum power transfer, the Thevenin equation for maximum power transfer was used:

$$P = \frac{V^2}{4R} \text{ (Equation A)}$$

where V is the estimated voltage generated and R is the terminal resistance of the motor. Voltage was estimated using

$$V = \frac{u}{K} \text{ (Equation B)}$$

with $u = 3150$ rpm the estimated rotor speed at 11 m/s and K the motor speed constant in rpm/V. This estimated power transfer was found to be highest for the Maxon RE 40. Due to a low speed-constant of 69.7 rpm/V, the voltage generated at 3150 rpm is expected to be 45.2 V, which is close to the nominal voltage of the motor of 48 V. Thus, we can expect the generator to operate close to the max efficiency of 89%.

To analyze the performance of the chosen generator in our system, we performed both theoretical analysis and experimental tests. For experimental testing, a 3D-printed snug cylindrical spool was press-fit onto the generator shaft and weights were attached to the spool to simulate an applied torque on the generator. The goal of this testing was to determine the optimal fixed-resistance load. With the torque input fixed, various resistance values were attached to the terminals of the generator and the power and shaft rpm were measured. A load resistance value of 30 Ω was found to produce the highest power and rpm for a given torque and thus was chosen as the load resistance (Figure 13).

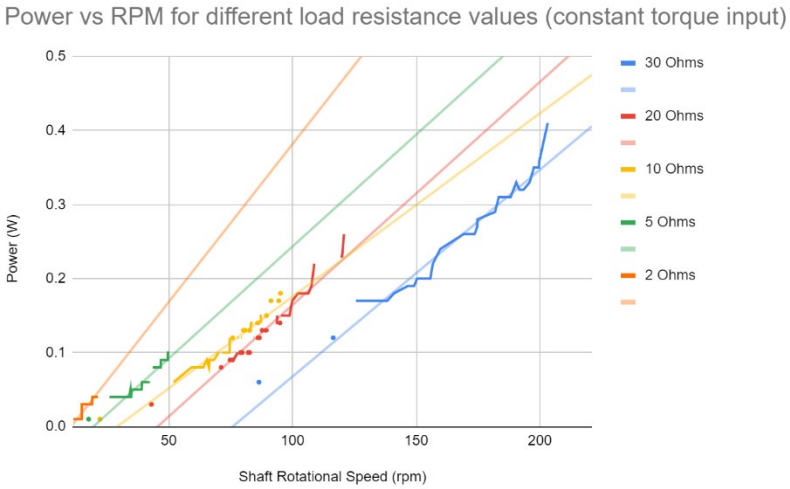

Figure 13: Power vs RPM for various load resistance values given a single torque input.

For the theoretical analysis, the relationship between shaft rpm, and voltage and current produced was examined. The voltage produced by the generator (U_i) is equivalent to the back EMF constant (K_e) times the RPM (ω). The total voltage (U_T) is defined as the following:

$$U_T = U_i - (R_{load} + R_{generator})I_{load} = K_e\omega - (R_{load} - R_{generator})I_{load}$$ (Equation C)

In a situation where the generator is short circuited with the load ($U_T = 0$), I_{load} would be at its maximum value and the equation looks like this:

$$K_e\omega = (R_{load} + R_{generator})I_{load}$$ (Equation D).

Our generator is rated for 1.4 A, therefore $I_{load} = 1.4$ A. Based on QBlade analysis, the maximum RPM is estimated to be 3150 at 11m/s wind speed. The generator's back EMF constant is 69.7 rpm/V. The generator resistance ($R_{generator}$) is 6.46 Ω. This information is used to calculate an appropriate load resistance (R_{load}) by rearranging Equation D. The load resistance was calculated to be at least 25.82 Ω. Thus, the experimentally derived resistance of 30 Ω fits in this range:

$$R_{load} = \frac{K_e\omega}{I_{load}} - R_{generator} \geq 25.82\ \Omega$$ (Equation E).

During shutdown and cut-in conditions the generator is disconnected from the normal and connected to a smaller, diversion load on the turbine-side of 17 Ω. When cutting in, the generator should only switch back over to the normal load when the normal load voltage will be at least 7 V in order to properly power the Arduino and linear actuator. The voltage across the 17 Ω diversion load that would produce a 7 V drop across the normal load was calculated to be 5.84 V.

The theoretical maximum voltage produced by the generator was calculated to be 45.19 V. However, the power sensors used in the circuit have a rated voltage of 40 V. In order to drop the voltage into the power sensor, a 4 Ω load was added. At max RPM, we will also be at max current, therefore the current through the load will be 1.4 A. The voltage drop across the 4 Ω load will be 5.6 V which is enough to drop the voltage to a safe level.

5.2 Power System Design

Due to the usage of a DC generator, there is no need for power rectification nor phase conversion, greatly simplifying the power system design and mitigating some power losses. A single-line diagram of the complete electrical system is shown in Figure 14.

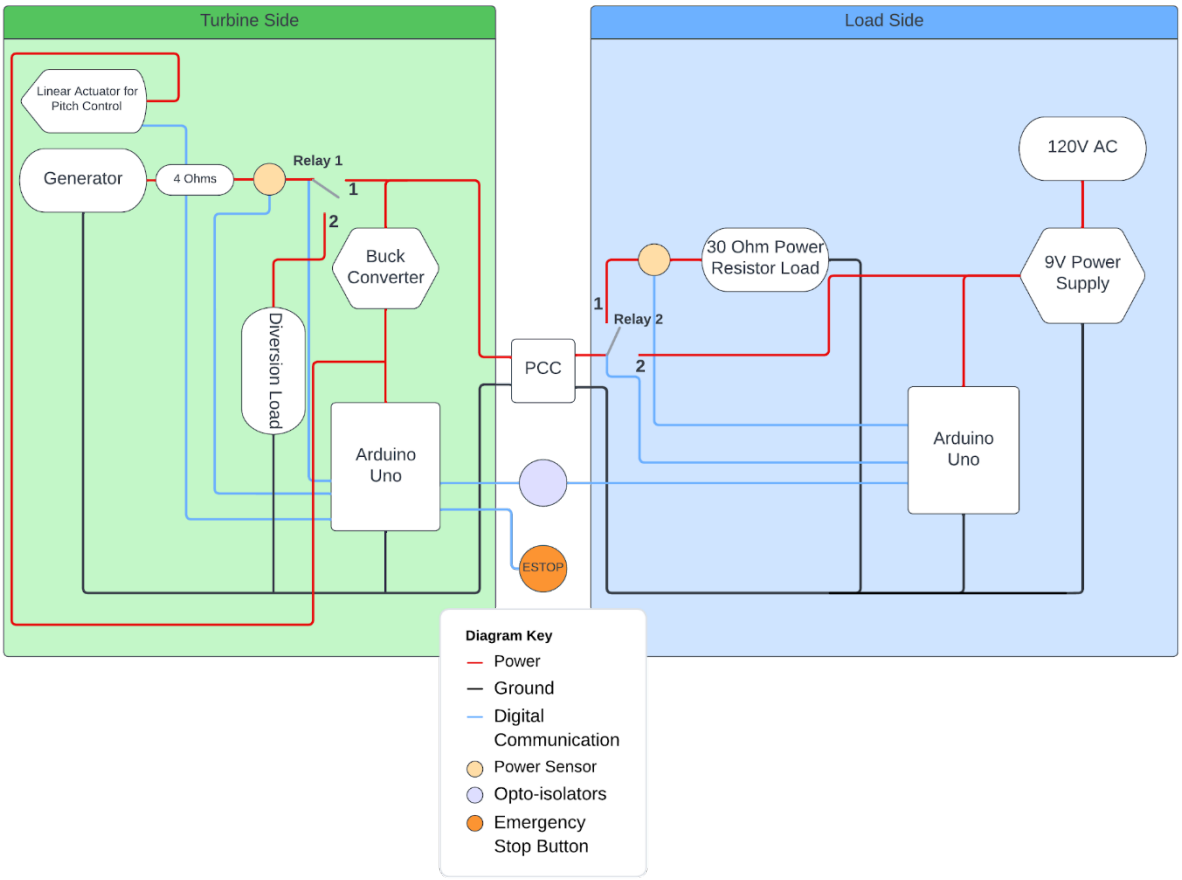

Figure 14: One Line Diagram of Complete Turbine and Load Electrical System.

Connected to the high-side of the generator are four-ohms of resistance, the INA260 power sensor, and a latching relay (Relay 1). The INA260 sensor was chosen over others because of its higher voltage rating and the specialized Arduino library, which simplifies implementation. The relay switches between connecting the generator to the turbine-side Arduino and PCC (position 1), and connecting the generator to a diversion load (position 2), which is used during shut-down and cut-in operations when the generator is not connected to the PCC. The relay is controlled by NPN bipolar transistors, whose inputs come from Arduino digital pins. The relay-transistor schematic is shown in Figure 15.

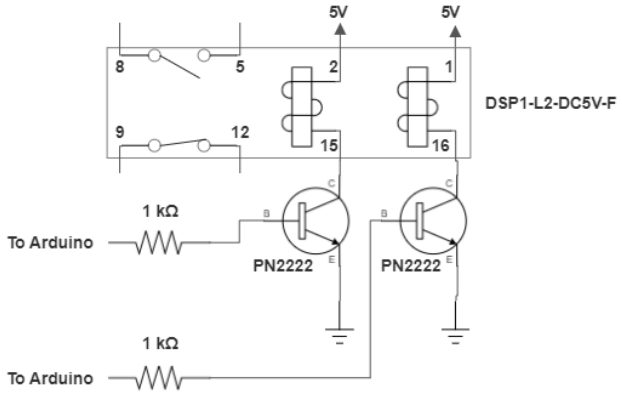

Figure 15: Schematic of latching relay control with bipolar transistors.

On the turbine-side the main power rail from the generator is connected to two parallel connections: one to the turbine-side Arduino and linear actuator and one to the PCC. To power the linear actuator and Arduino, power generated from the turbine is bucked down to 7 V using a buck converter.

On the load side, connected to the PCC is a latching relay (Relay 2) that switches between the turbine load and a 9V power supply. Because we are a relatively new team, we opted to use a fixed resistance load over a variable load in order to simplify the design, though a variable resistance load would allow for power optimization and regulation. The load, determined through testing, is 30 ohms. The load-side controls are powered by a 9V power supply with a wall plug, which plugs directly into the load-side Arduino and powers the turbine-side during safety shutdown and cut-in procedures.

5.3 Control System Design

The control system consists of two Arduino Uno boards, chosen due to familiarity with Arduino programming among the team. There is one Arduino board on turbine-side and one on the load-side, which use serial communication to communicate through an optically-isolated connection. A schematic of this connection is shown in Figure 16.

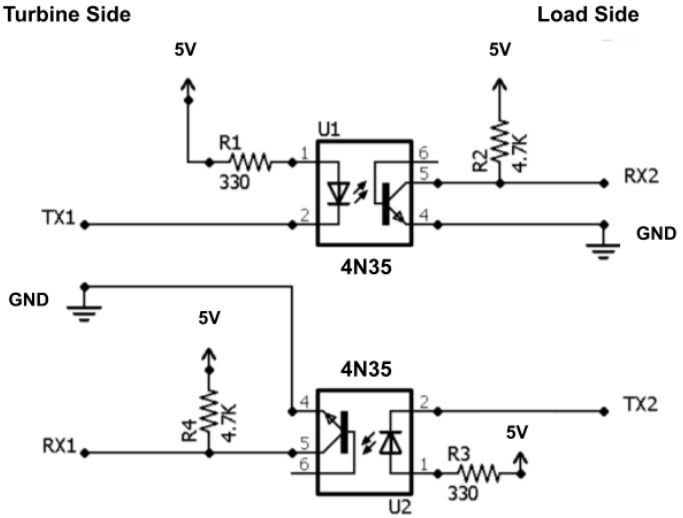

Figure 16: Optoisolator Schematic.

Turbine control will be based on which of four performance states (Cut-in, Normal Operation, Power Regulation, and Safety Shutdown) the turbine is operating in. Figure 17 gives a detailed state diagram describing the control operation. We sought to optimize pitch in each of the three pitch control states corresponding to the three of the four regimes of operation. These three regimes were cut-in (< 5 m/s), normal operational (5-11 m/s), power regulation (> 11 m/s). Because this was our first year in competition, we decided not to actively control pitch during the cut-in and normal operation sections of the competition. Instead, we determined the optimal cut-in and normal operation pitch through wind tunnel testing. Active pitch control was developed for the power-regulation task. In this state, blade pitch adjusts at small discrete time intervals in an attempt to maintain the maximum power achieved at wind speeds of 11 m/s during the power curve task.

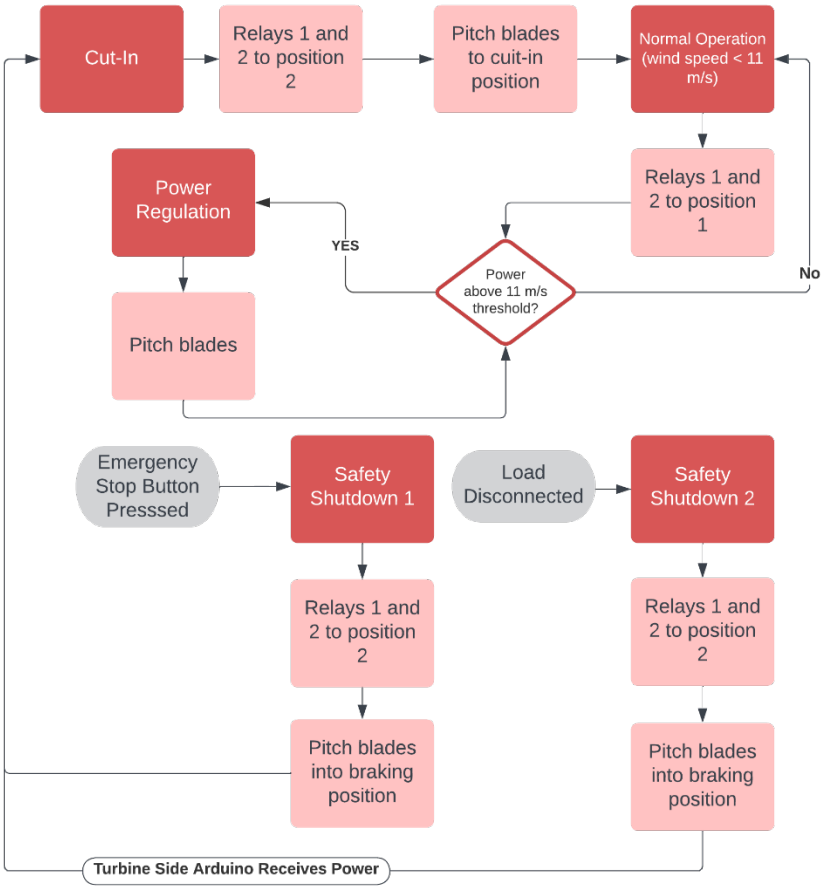

Figure 17: Control State Diagram.

The change in blade pitch is executed through commands sent by the turbine-side Arduino to the linear actuator control board. Servo control was determined to be the optimal linear actuator control method - out of either manual PWM, analog output PWM, or RC servo - due to ease of implementation and greatest consistency. Using the 'Servo.h' Arduino library, we were able to set the linear actuator position with a single digital output pin on the turbine-side

Arduino. Input values of 0 to 180 supposedly corresponded to full retraction and full extension, respectively, of the linear actuator. After testing, however, it was found that the range of 50 to 140 corresponded to full retraction and extension. Once the pitch change method was understood, we had to implement control logic and test.

The “perturb and observe” method was used to control the pitch of the blades during the power regulation task. An estimate of power produced by the turbine at 11 m/s wind speed was determined through testing in the campus wind tunnel. This estimate is used as a threshold to indicate when the wind speed has surpassed 11 m/s and the turbine should enter power regulation. In power regulation, wind speed will be increased, and the blades will have to pitch to maintain this power target. The logic during this task is to perturb the blades in a specified direction and observe whether the magnitude of the power difference between measured and target powers decreases following perturbation. If it decreases, the perturbation direction will remain the same, and the process will repeat. If the power difference magnitude increases, the perturbation direction will be flipped, and the process will repeat until the power difference is within a determined threshold.

Further wind tunnel testing was done to determine the optimal pitch angle for wind speeds of 5 m/s to 11 m/s (normal operation). To calculate the optimal pitch, we swept through all possible pitch angles at a wind speed of 5 m/s and measured power at each pitch. From this testing, the optimal angle was determined to be 65 degrees (Figure 18).

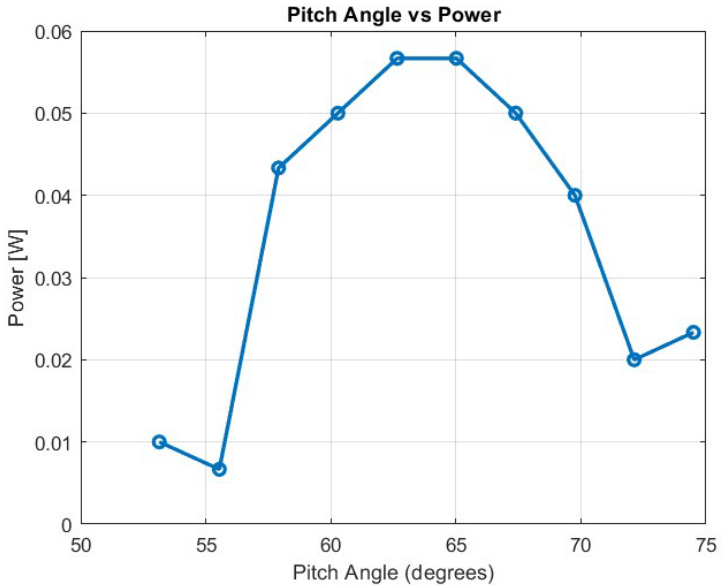

Figure 18: Varying Pitch Angle At 5m/s Wind Speed.

The control system was designed to account for two safety shutdown procedures: emergency stop button depression (ESTOP) and a load disconnection. To enter ESTOP shutdown, the turbine-side Arduino must receive a low signal from the ESTOP circuit. The turbine-side Arduino will then send a signal to the load-side Arduino to switch into emergency stop mode. Both relays are switched so that power now flows from the load-side to the turbine-side Arduino and the blades are pitched to braking position. When the emergency stop button is released, blades are pitched to cut-in, and both Arduinos switch back into normal operation when

power reaches the minimal threshold. The control system enters load disconnection when the load-side Arduino reads zero power from the load-side power sensor during normal operation or power regulation. The load-side Arduino signals to the turbine-side Arduino that a load-disconnect state has been entered. The blades are pitched to braking position and both relays are switched, causing the turbine-side Arduino to lose power. When load reconnection occurs, the turbine-side Arduino will boot up, pitch blades to cut-in position, and tell the controls to switch to normal operation when minimum threshold power is reached.

Testing of the control system was performed using a variable DC power supply in place of the generator. Behavior of the circuit, particularly of the relays whose position is indicative of the mode of operation, was observed as voltage increased (simulating cut-in), during the depression of an emergency stop button, and during a disconnection of the load and turbine sides. A driving dynamometer system was considered for testing, but due to the team's inexperience and lack of an existing design, it was decided that it would be more beneficial to focus efforts on turbine development.

6.0 Appendix 1: Unprocessed Results from Testing at 5m/s Wind Speed

Pitch Position	Pitch Angle	Average Voltage [V]	Average Power [W]	Average RPM
95	74.50	6.38	0.02	444.83
100	72.13	9.40	0.02	655.41
105	69.76	9.57	0.04	667.26
110	67.39	13.84	0.05	964.36
115	65.02	16.34	0.06	1138.84
120	62.65	17.47	0.06	1223.76
125	60.28	17.31	0.05	1206.24
130	57.91	12.78	0.04	890.71
135	55.54	4.21	0.01	293.12
140	53.14	2.33	0.01	162.23

7.0 Appendix 2: Assembly and Commissioning Checklist

Action	**Complete?**
Auger shafts placed through stops and holders and secured with hex nuts	
Foundation placed in tank and auger shafts rotated into sand	
Testing force applied to center column	
Stub attached to foundation	
Wires from tower passed through stub	
Stub screws threaded through tower base plate holes	
Generator secured in nacelle housing and wired directed through tower	
Nacelle shell housing screwed to nacelle base	
Nacelle secured to tower clamp and bearing	
Blades oriented into path of wind and clamp locked in place	
Turbine and load wires attached to PCC	
Emergency stop button connected to turbine-side circuit	
Load power plugged in	

References

[1] ASCE, "Minimum design loads for buildings and other," American Society of Civil Engineers., 2013.

[2] M. Keene, "Comparing offshore wind turbine foundations," Windpower, 4 January 2021. [Online]. Available: https://www.windpowerengineering.com/comparing-offshore-wind-turbine-foundations/. [Accessed 4 May 2023].

[3] B. W. Byrne and G. T. Houlsby, "Helical piles: an innovative foundation design option for offshore wind turbines," *Philosophical Transactions A,* vol. 373, no. 2035, 2015.